In situ observations of spiral growth on ice crystal surfaces

Ken-ichiro Murata,* Ken Nagashima, and Gen Sazaki
Institute of Low Temperature Science, Hokkaido University, N19-W8, Kita-ku, Sapporo 060-0819, Japan

(Received 14 June 2018; published 10 September 2018)

The spiral growth of crystals, mediated by their screw dislocations, is a general crystal-growth mechanism observed over a large variety of crystalline solids. Despite its general nature, direct observations of the spiral growth of ice have been rarely reported so far. Here, with the aid of advanced optical microscopy, we succeed in making *in situ* observations of the perfect spiral growth during the vapor growth of ice. We find that the spiral steps observed are well described by the classical Burton–Cabrera–Frank theory, taking into account surface diffusion of water admolecules between adjacent steps. This is distinct from the dominant growth mode that we have assigned as spiral in our recent studies, which accompanies fluctuations of the adjacent step interval. We also successfully capture the birth of a screw dislocation and the ensuing spiral growth, originating in the lattice mismatch arising from the coalescence of single ice crystals. Furthermore, we demonstrate that the nucleation of quasi-liquid layers (QLLs) takes place at the spiral center immediately after the birth of the dislocation, which suggests a link between screw dislocations and the generation of QLLs near the ice melting point.

DOI: 10.1103/PhysRevMaterials.2.093402

I. INTRODUCTION

Ice crystal formation is one of the essential processes linked to a diverse set of natural phenomena on earth, such as the formation of atmospheric clouds, precipitation, sea ice formation, frost heaving, ice accretion, and so forth [1]. It takes place not only via supercooled water but also directly from supersaturated water vapor, the latter of which is referred to as the vapor growth of ice. This process is known to be intimately related, for example, to the growth of ice crystals in mixed-phase clouds [2,3], causing the cold rain (the so-called Bergeron–Findeisen process [4]) and the rich morphological pattern of snow crystals, famously recorded in the Nakaya diagram [5]. In this context, the kinetics of ice crystal growth from supersaturated water vapor has historically attracted considerable attention.

It is generally established that the growth of faceted crystal surfaces proceeds layer by layer through nucleation and growth of two-dimensional (2D) islands, and/or spiral growth triggered by screw dislocations. Importantly, the latter is a barrierless process, governing the growth of crystals in a low supersaturation regime where 2D nucleation is almost impossible stochastically. The relevance of this picture has been checked for many years both theoretically and experimentally, regardless of the system [6,7]. For practical applications, it is also worth noting that spiral growth plays a key role in making high-quality protein crystals [8]. This growth mode is known to rather suppress incorporation of impurities into crystals, compared with the 2D nucleation growth mode. Moreover, fairly recently, Tominaga *et al.* offered a new approach, facilitating the growth of protein crystals by inducing screw dislocations (i.e., the spiral growth) with laser ablation [9].

Due to its general nature, spiral growth is also expected to be common in ice crystals. However, direct visualizations of elementary spiral steps on ice crystal surfaces are rare. This is mainly due to the small reflectivity of ice-air and ice-water interfaces (1.8% and 0.01%, respectively). Only recently have Thürmer and Nie [10] succeeded in making direct observations of elementary spiral steps using scanning tunneling microscopy and atomic force microscopy. Although they uncovered the step structure and its link to the morphological selection between cubic ice (I_c) and hexagonal ice (I_h), they did not shed light on the thermodynamic aspects of spiral growth because of limited experimental conditions (temperatures lower than 140 K under extremely low vapor pressure, fixed below 3×10^{-11} mbar [10]).

In our recent series of studies [11–14], we made *in situ* observations of ice crystal growth by using advanced optical microscopy (laser confocal microscopy combined with differential interference contrast microscopy: LCM-DIM), whose resolution in the height direction reaches the order of an angstrom [11,15]. We investigated the elementary step dynamics on ice crystal surfaces under well-controlled temperatures and water vapor pressures. Even in our *in situ* observations at the level of elementary steps, however, no perfect spiral growth has been confirmed on ice crystal surfaces so far, contrary to the 2D nucleation and growth. While we have often observed a growth mode reminiscent of spiral growth, accompanying double (paired) bilayer-like steps [12], this exhibits significant fluctuations in the distance between adjacent steps [14] and its spiral center is always located at edges or outside of facets. Strictly speaking, it is fair to say that the thermodynamic nature of spiral growth on ice crystal surfaces still remains unclear at this stage.

In this article, we present several examples of observations of the genuine spiral growth on ice basal faces with the aid of LCM-DIM. We succeeded in making direct visualization of advancing spiral steps born from screw dislocations formed by

*murata@lowtem.hokudai.ac.jp

coalescence of single ice crystals. We discuss quantitatively the detailed relationship between this spiral behavior and the Burton–Cabrera–Frank (BCF) theory [16,17], the classic model for spiral growth. Furthermore, we also demonstrate that such screw dislocations not only mediate the spiral growth itself, but also assist the formation of quasi-liquid layers (QLLs) near the melting point of ice. Our findings offer a fundamental understanding of the origin of ice crystal growth from water vapor, inseparably involved in the unsolved conundrum of the complex behavior of the ice crystal habit [5,18].

II. METHODS

In this study, we employed a confocal system (FV300, Olympus Corporation) attached to an inverted optical microscope (IX70, Olympus Corporation) with a superluminescent diode (Amonics Ltd., model ASLD68-050-B-FA, 680 nm) as a light source to prevent the generation of interference fringes. In the observation images, the differential interference (DI) contrast was adjusted as if the ice crystal surface were illuminated by a light beam slanted from the upper-left to the lower-right direction. Thus, convex (concave) objects showed brighter (darker) and darker (brighter) contrast on the upper-left sides and the lower-right sides, respectively, compared with a flat crystal surface.

An observation chamber is composed of upper and lower Cu plates, whose temperatures were separately controlled by using Peltier elements. At the center of the upper Cu plate, a cleaved AgI crystal was attached as an ice nucleating agent. Sample ice crystals were grown epitaxially on this AgI substrate. Other ice crystals were also prepared on the lower Cu plate, as a source of water vapor for the sample ice crystals. The vapor pressure in the chamber is controlled by the temperature of the source ices; that is, their equilibrium vapor pressure at the corresponding temperature because a larger amount of source ice is attached to the lower plate compared with the sample crystals on the upper plate. Thus, separate control of the temperature of the sample and source ice crystals allows us to adjust the temperature (T) and water vapor pressure (p) of the sample independently. Here, p is the partial pressure of H_2O in a nitrogen environment. The total pressure is the atmospheric pressure. For the discussion below, we further define supersaturation of ice crystals as $\sigma = (p - p_e)/p_e$, where p_e is the equilibrium water vapor pressure for the sample ice.

We used ultrapure water (>18.2 MΩ cm) as a source of ice and vapor. The purity of dry nitrogen gas filling the observation chamber is more than 99.99 % (oxygen $\leqslant$50 vol. ppm and the dew point $\leqslant -58\,^{\circ}$C). Further details of the experiments are described in Refs. [11,19].

III. RESULTS AND DISCUSSION

Figure 1(a) shows an observation example of spiral growth of an ice basal face visualized by LCM-DIM ($T = -9.7\,^{\circ}$C and $p = 280$ Pa). We see that steps rotate around a trench (a gap between the two sides of the prismatic walls) and steadily flow in the counterclockwise direction while keeping an equal step spacing, which is characteristic of the spiral growth behavior. However, this spiral pattern does not coincide with that of a simple spiral stemming from a single screw dislocation. To clarify the origin of this step behavior, in Fig. 1(b) and 1(c) (also in Videos S1 and S2 [20]), we follow the birth of the spiral steps by tuning the water vapor pressure from an equilibrium value [$\sigma \sim 0$; Fig. 1(b)] to supersaturation [$\sigma > 0$; Fig. 1(c)]. Initially, we see a single stationary step in the equilibrium region [see the green arrow in Fig. 1(b)]. Soon after entering the supersaturation regime, this single step starts to rotate and simultaneously splits up into lower steps [Fig. 1(c)]. Next, these spirals reach the steady growth state shown in Fig. 1(a) (see also Videos S1 and S2 [20]). As discussed below, these splitting steps correspond to the elementary steps in light of the step velocity. We find that the sum of the splitting steps is fourteen,

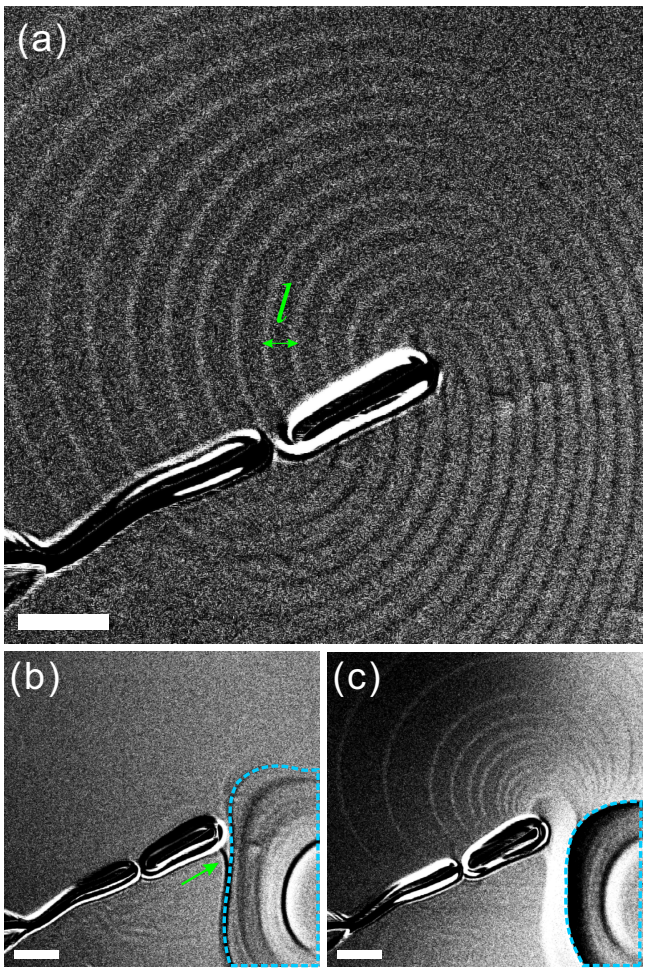

FIG. 1. (a) LCM-DIM image of spiral growth on an ice basal face at $T = -9.7\,^{\circ}$C and $p = 280$ Pa. The contrast of the spiral steps is enhanced by subtracting the averaged background image. Here, l corresponds to the step spacing. (b) The ice basal face at $T = -9.7\,^{\circ}$C and $\sigma = 2.4 \times 10^{-3}$ ($p = 268$ Pa). The area enclosed by the blue dashed line indicates the undersaturated region and is hollowed by sublimation (see the DI contrast opposite to the steps, meaning the concave surface). This ice surface has a very weak gradient of the water vapor pressure. The thick step shown by the green arrow is stationary at the boundary between supersaturation and undersaturation where σ is exactly zero. The height of this step corresponds to the magnitude of the Burgers vector. (c) At $T = -9.7\,^{\circ}$C and $\sigma = 0.039$ ($p = 277$ Pa). The white bars are 20 μm.

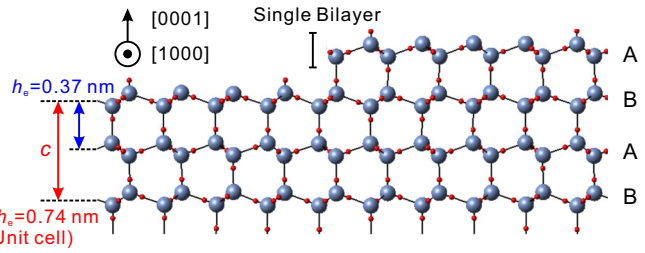

FIG. 2. Schematic illustration of a cross section of a hexagonal ice crystal and its elementary step. Gray and red atoms correspond to oxygen and hydrogen, respectively.

which tells us that the magnitude of the Burgers vector of the screw dislocation, $|\boldsymbol{b}| = b$, in this system corresponds to the height of the fourteen elementary steps, $14h_e = 5.28$ nm ($h_e = 0.37$ nm being the height of the elementary step; see Fig. 2).

As shown in Fig. 2, on the basal face of the hexagonal ice, the minimum component of the Burgers vector of screw dislocations is the double-bilayer height; that is, the unit-cell height in the direction of the c axis ($2h_e = 0.74$ nm), because of the crystallographic restriction to keep the periodic ABAB stacking consequence. Due to the entropic gain, such double-bilayer steps further split up into two single bilayers (A and B components, respectively), flowing alternately on surfaces as observed in many systems [21–23]. Thus, the elementary step in this system corresponds to this single bilayer (A or B) and the height of the fourteen elementary steps is that of seven unit cells. Here, note that the single bilayer steps A and B are equivalent in this temperature range because the steps already undergo a step-roughening transition (see the circular shape of the steps in Fig. 1). Furthermore, due to the crystallographic periodicity, the number of the spiral steps generated from a dislocation is restricted to an even number, which is satisfied in this system.

How is the screw dislocation formed in this system? In Figs. 3(a)–3(d), we show a schematic of its formation process. As observed in Fig. 3(e), we see the presence of a trench, generated by the coalescence of two single crystals. Under supersaturated conditions, the side walls (the prismatic faces) of the trench grow and finally attach to each other at a certain position. If there exists a gap in the height between both sides, this leads to a lattice mismatch in the normal direction to the surface, resulting in the screw dislocation. Actually, we confirm a seam of the trench, corresponding to the attachment point [see the arrow in Fig. 3(b)]. The step with the height of b, although instantaneously splitting into multiple elementary steps, starts to rotate with a finite curvature and steadily grows while passing through the seam [see Fig. 3(f) and Videos S1 and S2 [20]]. Note that this mechanism has been recognized as one of the prominent routes to yield screw dislocations; for example, as discussed by Chernov [6].

In Fig. 4, we show the σ dependence of the step-advancing velocity v_{st} at $T = -9.7\,^{\circ}$C as an example. At higher σ, v_{st} slightly deviates from the simple linear relation between the step velocity and supersaturation ($v_{st} \propto \sigma$) expected from the standard crystal-growth theory [6]. This deviation from linear comes from the depletion of water vapor due to the surrounding

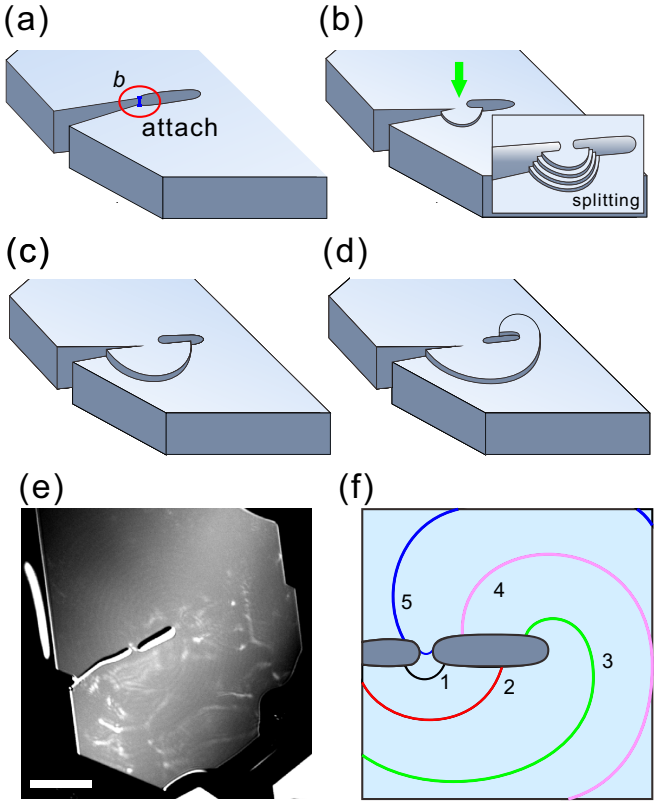

FIG. 3. (a)–(d) A schematic of the birth of the screw dislocation and the resulting spiral growth. The green arrow shows a seam, generated by the growth of the side walls in the trench. The inset in panel (b) shows an example of the step splitting. Here, the number of the splitting steps is four, not fourteen, for convenience. (e) The whole image of the ice crystal surface observed in Fig. 1. The white bar is 50 μm. (f) Schematic of the motion of a single step during the spiral growth in this system. The surface steadily grows in the circular process of 1–5.

ice crystals growing together with the target ice [13,14]. For practical convenience, we employ here $v_{st}(\sigma) = v_{st}^{\infty} \tanh(\alpha\sigma)$ as a fitting function (the red line in Fig. 4), where α is a constant and v_{st}^{∞} is a saturated step velocity at $\sigma \to \infty$ (the depletion limit). Note that the term of $\tanh(\alpha\sigma)$ does not come from the step-step interaction of the BCF theory.

While ice surfaces experience a lower supersaturation (hereafter defined as σ_s) than that in the atmosphere inside the chamber (σ) at higher σ, such depletion is absent at the lower limit of σ (see the clear linearity near $\sigma = 0$ in Fig. 4). Thus, the step velocity without depletion is given by the first-order expansion of $v_{st}(\sigma)$ at $\sigma = 0$; that is, $v_{st} = v'_{st}(\sigma = 0)\sigma = \alpha v_{st}^{\infty}\sigma$ (the blue line in Fig. 4), where the proportionality factor αv_{st}^{∞} is the so-called step kinetic coefficient in this system. Here, note that the supersaturation at the ice surface σ_s satisfies this linear relation: $v_{st} = \alpha v_{st}^{\infty}\sigma_s$. Therefore, as shown in Fig. 4, once v_{st} is given at a certain σ, σ_s can be experimentally determined as $v_{st}/\alpha v_{st}^{\infty}$, which is reduced from σ. In this system, contrary to our previous studies [13,14], we can access extremely low supersaturated regimes ($\sigma \sim 0.01$), exhibiting no depletion effects (see also inset in Fig. 4), because we are able to observe the spiral center inside the facet directly, which

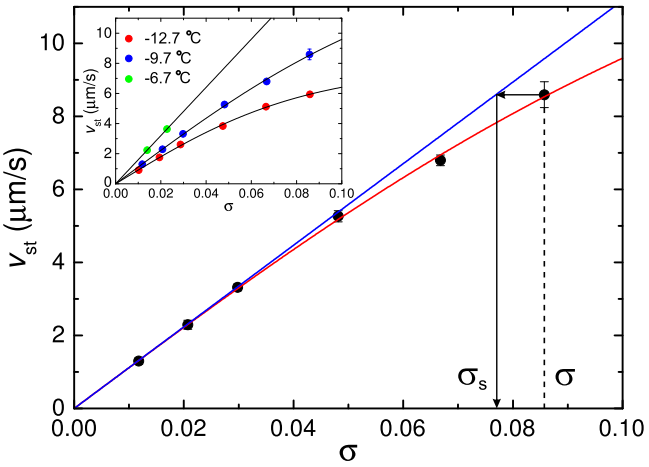

FIG. 4. The supersaturation (σ) dependence of v_{st} at $-9.7\,^{\circ}$C. The red line indicates the fit with $v_{st} = v_{st}^{\infty}\tanh(\alpha\sigma)$, including water vapor depletion at the surface whereas the blue line shows the prediction with the absence of depletion, $v_{st} = \alpha v_{st}^{\infty}\sigma$. Note that σ_s is given by $v_{st}(\sigma)/\alpha v_{st}^{\infty}$. The inset shows v_{st} for different temperatures. From the fit, we obtain $\alpha = 7.15$ and $v_{st}^{\infty} = 15.6$ μm/s ($-9.7\,^{\circ}$C) and $\alpha = 7.74$ and $v_{st}^{\infty} = 11.8$ μm/s ($-12.7\,^{\circ}$C). For $T = -6.7\,^{\circ}$C, we employ a simple linear fit because of the lack of data at higher σ (the slope is 160 μm/s).

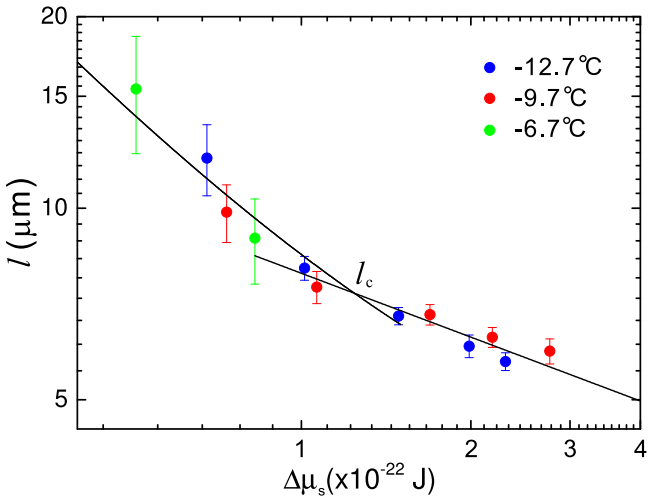

FIG. 5. Scaling relation between l and $\Delta\mu_s$ for different temperatures. Here, l_c correspond to a characteristic step spacing where the crossover of the scaling exponent takes place.

allows us to discuss the thermodynamic nature of the spiral growth much more precisely.

The inset in Fig. 4 shows the data for v_{st}, further including the cases of $T = -12.7\,^{\circ}$C and $-6.7\,^{\circ}$C. We can see the depletion effect at $-12.7\,^{\circ}$C as well as at $-9.7\,^{\circ}$C, although it cannot be confirmed at $-6.7\,^{\circ}$C due to the lack of data at higher σ. Here, we estimate the step kinetic coefficient, described as $v_{st}'(0) = \alpha v_{st}^{\infty}$ in our expression, at each temperature. As a result of the fitting analysis, we obtain the step kinetic coefficients of 91.3 μm/s ($-12.7\,^{\circ}$C), 112 μm/s ($-9.7\,^{\circ}$C), and 160 μm/s ($-6.7\,^{\circ}$C); the values of which almost agree with those of the elementary step quite recently obtained by us [14]. Thus, the splitting spiral step shown in Fig. 1 can be regarded as the elementary step.

To check the relevance of the BCF picture for the spiral growth on ice surfaces, we also examine the relationship between the step interval l [see Fig. 1(a)] and the surface chemical-potential difference between ice and water vapor (the driving force in this system), $\Delta\mu_s$. The latter quantity can be defined by σ_s as $\Delta\mu_s = k_B T \ln(1+\sigma_s)$, where k_B is the Boltzmann constant. Figure 5 indicates the $\Delta\mu_s$ dependence on l at $T = -12.7\,^{\circ}$C, $-9.7\,^{\circ}$C, and $-6.7\,^{\circ}$C. The data show a nice collapse among the different temperatures, which means that the step free energy of the ice basal face is independent of T in this temperature regime. We see that two characteristic regimes exist at lower $\Delta\mu_s$ and higher $\Delta\mu_s$. In the former region, due to the broad step spacing, surface diffusion effects on adjacent steps are absent. Thus, the following well-known relation of the spiral growth [24] is expected to appear:

$$l_s = 19\Omega\kappa(\Delta\mu_s)^{-1}, \tag{1}$$

where l_s is the step interval of a single spiral, κ is the step free energy of the ice basal face, and Ω is the surface area occupied by one water molecule (8.85×10^{-20} m^2 for the basal face).

However, as discussed above, the spiral steps observed are not a single spiral but are composed of fourteen splitting steps. This spiral pattern is exactly reminiscent of that generated from a group of multiple dislocations with the same sign, evenly ordered in a straight line [25,26]. Given the length of the straight line (here, the length of the trench) and the number of the dislocations as L and n, respectively, the resultant interstep spacing is known to be expressed as follows [25]:

$$l = \frac{l_s}{n(1+2L/l_s)^{-1}}, \tag{2}$$

where $L = 39$ μm and $n = 14$ in this system. Note that, although Burton *et al.* employed $l_s = 4\pi\Omega\kappa(\Delta\mu_s)^{-1}$ in their original paper [25], we employ here the more accurate form of $l_s = 19\Omega\kappa(\Delta\mu_s)^{-1}$ [see Eq. (1)] derived by Cabrera and Levine [24]. From fitting Eq. (2) to the data in the lower-σ regime, we obtain $\kappa = 4.7(\pm 0.2) \times 10^{-9}$ J/m, the value of which agrees well with that recently determined from the observation of imperfect spiral growth ($\kappa = 5.0 \times 10^{-9}$ J/m) [14]. This suggests that κ estimated here, a quantity that is extremely difficult to determine in the usual manner, is sufficiently robust.

On the other hand, the latter region exhibits a rather moderate change in l [$\propto(\Delta\mu_s)^{-1/3}$]. This exponent is characteristic of the so-called back-force effect [27–31], appearing when the local supersaturation at a spiral center is depleted by the rest of the own (outer) spiral step. This crossover behavior is natural, considering the analogy to the back-force effect; that is, the competition between the step spacing and the surface diffusion distance λ_s, the value of which was previously estimated to be 4.5 μm [13]. The system is expected to recover the ideal spiral behavior [see Eqs. (1) and (2)] free from the depletion effect, when l reaches $2\lambda_s$ with decreasing $\Delta\mu_s$. This means that the spiral center is no longer influenced by the depletion of water vapor caused by adjacent steps. Actually, we find that $l_c \sim 7.3$ μm, where the crossover takes place, roughly corresponds to $2\lambda_s$. A similar crossover behavior, although indirectly characterized by the slope of hillocks, has

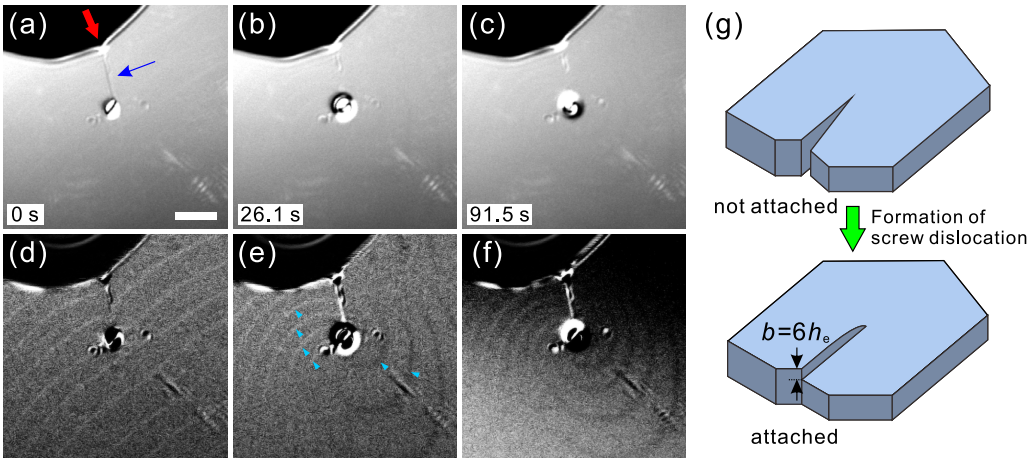

FIG. 6. (a)–(c) The birth of a screw dislocation and a resulting hollow core, and subsequent nucleation of a QLL ($T = -3.9\,^{\circ}$C and $p = 471$ Pa; see also Video S3 [20]). In this process, the transformation of the growth mode into the spiral growth also occurs simultaneously due to the formation of the screw dislocation. The white bar is 10 μm. (d), (e) Enhanced images of (a)–(c), obtained by the same procedure as Fig. 1 (see also Video S4 [20]). The light-blue arrowheads in panel (e) indicate the spiral steps flowing out from the core. (g) Schematic of the formation of the screw dislocation as shown in panels (a) and (b), viewed from the direction of the red arrow in panel (a).

been observed in solution growth systems [32–34]. Here, it is worth noting that, differently from the usual back-force effect, focusing on the single spiral step, the depletion of the supersaturation at an spiral center results not only from the rest of the own spiral step but also from adjacent splitting steps in this system. Even so, the characteristic exponent and its crossover themselves qualitatively agree with the conventional model of the back-force effect, which may imply that local depletion caused by multiple splitting steps roughly corresponds to that by a single spiral step with a narrower step spacing. However, in this system, an analytical form of l in the back-force regime ($l \leqslant 2\lambda_s$) still remains elusive. Because of the coupling between multiple splitting steps and the back-force effect caused by them, l cannot be written by the simple substitution of l_s under the back-force effect, $l_s = 5.32(T\Omega\kappa\lambda_s^2)^{1/3}(\Delta\mu_s)^{-1/3}$ (T being the tapering factor) [30,31], into Eq. (2). The theoretical approach taking into account this coupling properly is highly required in the future.

We next focus on the relationship between screw dislocations and the generation of QLLs near the ice melting point. Figure 6 and Videos S3 and S4 [20] show the transformation of the growth mode into the spiral growth and subsequent nucleation of a QLL from a spiral center; that is, a hollow core. Before the transformation, we see a clear grain boundary at the top of the hollow core [see the blue arrow in Fig. 6(a)]. The spiral growth begins to proceed immediately after the disappearance of the grain boundary by the attachment of the neighboring facets [Figs. 6(b) and 6(e)]. This clearly indicates that lattice mismatching, resulting in the screw dislocation, takes place by this coalescence as schematically shown in Fig. 6(g). On this surface, we can see six spiral steps flowing out from the hollow core, which means that the magnitude of the Burgers vector of this screw dislocation corresponds to the height of six elementary steps [see the arrowheads in Fig. 6(b)], $6h_e = 2.22$ nm, (the three unit cells in the direction of the c axis). In the initial process, the existing core grows as a result of the release of the strain energy associated with the screw dislocation [Fig. 6(b)], which can also be regarded as the process compensating for the strain energy by the surface energy (making the outcrop on the surface). Then, the hollow core is filled with a QLL nucleated and grown from the inside [Fig. 6(c)]. Here, interestingly, the spiral growth can survive even after the appearance of QLLs in the core [Fig. 6(f)], which implies that this growth mode is also expected to exist in the so-called melt growth of ice crystals.

This result suggests that the hollow core acts as a source of nucleation of QLLs. Note that the hollow core still stores the excess strain energy and also has a different surface free energy from the basal face, both of which generally affect the so-called heterogeneous nucleation. However, strain effects from solid substrates are not coupled to the energy barrier for the nucleation of QLLs due to the disordered nature of liquid, unlike the heteroepitaxy of solids [35]. In contrast, the surface free energy of ice is directly linked to the nucleation barrier through the wettability of QLLs on ice surfaces. Recently, we confirmed that the nucleation behavior of QLLs on a prism and other higher-index faces is almost identical to that on a basal face [36], which means that there is no significant difference in the surface free energy between the basal and the higher-index faces. Thus, the reduction of the nucleation barrier on the hollow core is extremely small even though it ideally exists.

The other possible origin of the nucleation of the QLL is the abrupt change in local supersaturation inside the hollow core, caused by its formation. We have demonstrated that the formation of the QLLs takes place not at the ice-vapor equilibrium but under certain supersaturated conditions (at least, beyond the metastable ice-water equilibrium line) [37,38]. Because, as shown in Fig. 6(b), a large amount of ice sublimes instantaneously due to the surface destabilization by the screw dislocation, this leads to a drastic increase in the local supersaturation and is sufficient to trigger the nucleation of QLLs.

Here, it is worth remarking on the relationship between screw dislocations and hollow cores. It is known that the hollow core formation occurs not only at undersaturation (the etch pit) but at supersaturation when the screw dislocation stores a

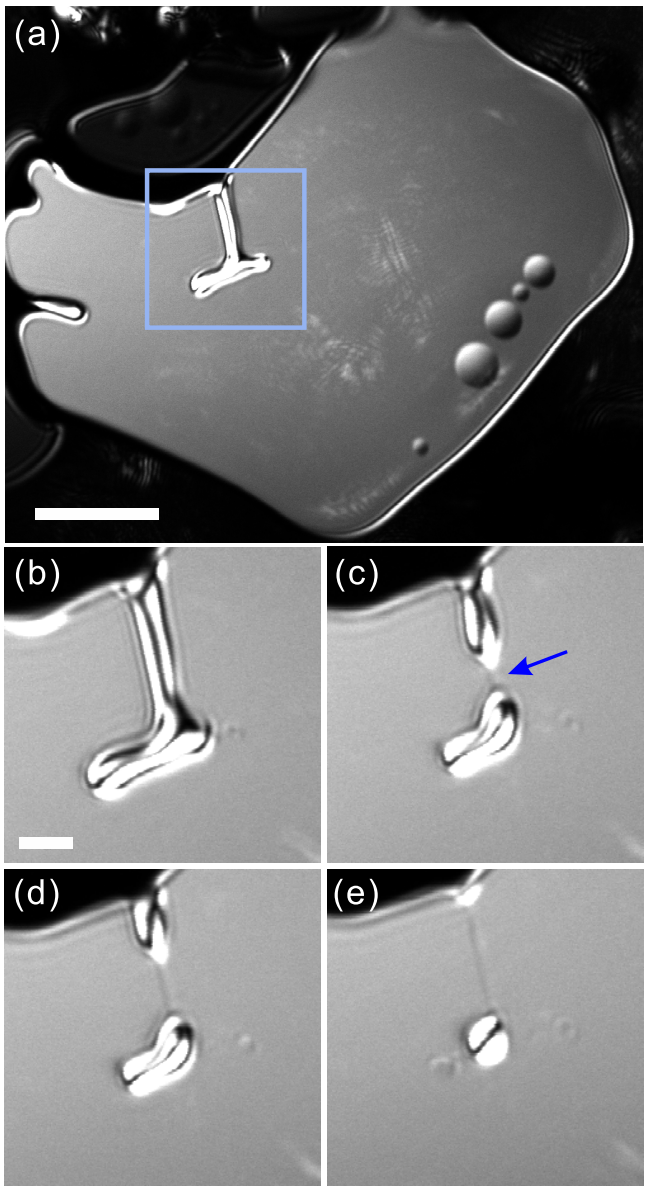

FIG. 7. The whole pathway to the formation of the grain boundary shown in Fig. 6. Here, the temperature is fixed at $T = -4.1\,^{\circ}\mathrm{C}$. (a) A whole image of the ice basal face at $p = 449$ Pa. The white bar is 50 μm. (b) $p = 438$ Pa. The white bar is 10 μm. (c) $p = 427$ Pa. (d) $p = 420$ Pa. (e) $p = 472$ Pa. Here, the time interval between panels (c) and (d) is 193 s. In panel (a), droplet-type QLLs already appear near the edge of the crystal, which may come from the heterogeneity of supersaturation (the so-called Berg effect); that is, the edge has higher supersaturation than the center.

sufficient strain energy density; that is, has a large Burgers vector [39]. The size of the hollow core, r_{hc}, is known to be described by b as $r_{\mathrm{hc}} = Gb^2/8\pi^2\gamma$ [40], where G is the shear modulus of ice ($\sim$3 GPa [41]) and γ is the surface free energy of the lateral side of the core ($\sim$0.1 J/m^2 [42]). In this equation, r_{hc} is referred to as the so-called Frank's radius. Inserting $b = 2.22$ nm, directly determined from Figs. 6(e) and 6(f), yields $r_{\mathrm{hc}} = 2$ nm, which means that the radius of the hollow core (almost 5 μm in Fig. 6) is too large compared with the Frank's radius. Surprisingly, this core size, reaching a micrometer scale, is comparable with that of SiC [43], which possesses a fairly high shear modulus ($\sim$200 GPa [44]). Although we cannot make any conclusive statement at this stage, the anomalous gap between the core size and the Burgers vector is an interesting topic to be addressed in the future.

Finally, we briefly follow how the above grain boundary [indicated by the blue arrow in Fig. 6(a)], acting as the source of the screw dislocation, is formed in a single ice crystal. In Fig. 7(a), we initially see a trigeminal trench (still not attached to each other), a vestige of merging of at least two single crystals. The trench shrinks due to growth of the side of the faces and the minimization of their surface free energies [Fig. 7(b)]. At a certain time, the neighboring faces attach to each other at one point [see blue arrow in Fig. 7(c)] and then the trench is gradually closed as a grain boundary while the hole remains inside [Figs. 7(d) and 7(e)]. Together with the observation in Fig. 1, the coalescence of crystals, leading to the lattice mismatching, is a prominent route to yield screw dislocations and the resulting spiral growth for ice crystal surfaces although coalescence is a rare event in our single ice crystals, grown epitaxially and in isolation on an AgI substrate. However, we speculate that spiral growth is more frequently observed on surfaces of polycrystalline ices, which inevitably include large numbers of dislocations and grain boundaries.

IV. CONCLUSIONS

With the aid of LCM-DIM, we succeed in making *in situ* observations of genuine spiral growth mediated by screw dislocations on ice basal faces. We have demonstrated that the spiral growth on ice is well described by the classical BCF theory, taking into account the depletion of water admolecules by adjacent steps. In fact, we have confirmed the crossover behavior in the step spacing, which is due to the presence or absence of the depletion. In our system, screw dislocations are formed through the lattice mismatch caused by the coalescence of neighboring single ice crystals, which is a common route to yield screw dislocations. Furthermore, we have also elucidated the relationship between hollow cores, generated by screw dislocations, and the formation of QLLs. Our noninvasive approach with optical microscopy has a great advantage for observing surfaces near the melting point, which is sensitive to the contact required by probe-based techniques, inevitably disturbing their native state.

We again note that the spiral growth presented in this article is distinct from the growth mode that we have often seen and assigned as spiral growth in our series of recent studies [11–14], exhibiting large fluctuations of the adjacent step interval with decreasing supersaturation. Such fluctuation effects are not dealt with by the simple spiral growth model described by BCF theory. This may imply the presence of other growth mechanisms, such as steady step nucleation excited by thermal fluctuations, although its origin is unclear at this stage. In addition, it still remains elusive why the source of their steps only appears at edges or the outside of facets. On isolated single ice crystals without coalescence, this apparent spiral growth is a dominant growth mode. Understanding the differences from the usual spiral growth is an important topic for future studies.

ACKNOWLEDGMENTS

The authors are grateful to Y. Saito and K. Ishihara (Olympus Corporation) for their technical support for LCM-DIM and G. Layton (Northern Arizona University) for the provision of AgI crystals. This work was partially supported by a Japan Society for the Promotion of Science Grant-in-Aid for Young Scientists (A) (Grant No. JP16H05979) and Scientific Research (A) (Grant No. JP15H02016).

[1] *Ice Physics and the Natural Environment*, edited by J. S. Wettlaufer, J. G. Dash, and N. Untersteiner (Springer-Verlag, Berlin, Heidelberg, 1999).
[2] H. Morrison, G. de Boer, G. Feingold, J. Harrington, M. D. Shupe, and K. Sulia, Nat. Geosci. **5**, 11 (2012).
[3] I. Tan, T. Storelvmo, and M. D. Zelinka, Science **352**, 224 (2016).
[4] T. Bergeron, in *Proc. 5th Assembly U.G.G.I.* (International Union of Geodesy and Geophysics, Lisbon, Portugal, 1935), pp. 156–180.
[5] U. Nakaya, *Snow Crystals* (Harvard University Press, Cambridge, 1954).
[6] A. A. Chernov, *Modern Crystallography III* (Springer-Verlag, Berlin, Heidelberg, 1984).
[7] A. A. Chernov, J. Cryst. Growth **264**, 499 (2004).
[8] M. Sleutel, G. Sazaki, and A. E. S. V. Driessche, Cryst. Growth Des. **12**, 2367 (2012).
[9] Y. Tominaga, M. Maruyama, M. Yoshimura, H. Koizumi, M. Tachibana, S. Sugiyama, H. Adachi, K. Tsukamoto, H. Matsumura, K. Takano, S. Murakami, T. Inoue, H. Y. Yoshikawa, and Y. Mori, Nat. Photonics **10**, 723 (2016).
[10] K. Thürmer and S. Nie, Proc. Natl. Acad. Sci. USA **110**, 11757 (2013).
[11] G. Sazaki, S. Zepeda, S. Nakatsubo, E. Yokoyama, and Y. Furukawa, Proc. Natl. Acad. Sci. USA **107**, 19702 (2010).
[12] G. Sazaki, H. Asakawa, K. Nagashima, S. Nakatsubo, and Y. Furukawa, Cryst. Growth Des. **14**, 2133 (2014).
[13] H. Asakawa, G. Sazaki, E. Yokoyama, K. Nagashima, S. Nakatsubo, and Y. Furukawa, Cryst. Growth Des. **14**, 3210 (2014).
[14] M. Inomata, K. Murata, H. Asakawa, K. Nagashima, S. Nakatsubo, Y. Furukawa, and G. Sazaki, Cryst. Growth Des. **18**, 786 (2018).
[15] G. Sazaki, T. Matsui, K. Tsukamoto, N. Usami, T. Ujihara, K. Fujiwara, and K. Nakajima, J. Cryst. Growth **262**, 536 (2004).
[16] F. C. Frank, Discuss. Faraday Soc. **5**, 48 (1949).
[17] W. K. Burton, N. Cabrera, and F. C. Frank, Nature (London) **163**, 398 (1949).
[18] T. Kobayashi, Philos. Mag. **6**, 1363 (1961).
[19] G. Sazaki, S. Zepeda, S. Nakatsubo, M. Yokomine, and Y. Furukawa, Proc. Natl. Acad. Sci. USA **109**, 1052 (2012).
[20] See Supplemental Material at http://link.aps.org/supplemental/10.1103/PhysRevMaterials.2.093402 for videos of the birth of elementary spiral steps (Video S1) and its contrast enhanced version (Video S2), and for videos of the nucleation of a QLL associated with the birth of a screw dislocation (Video S3) and its contrast enhanced version (Video S4).
[21] B. van der Hoek, J. P. van der Eerden, and K. Tsukamoto, J. Cryst. Growth **58**, 545 (1982).
[22] C. Stoica, W. J. P. van Enckevort, H. Meekes, and E. Vlieg, J. Cryst. Growth **299**, 322 (2007).
[23] A. G. Shtukenberg, Z. Zhu, Z. An, M. Bhandari, P. Song, B. Kahr, and M. D. Ward, Proc. Natl. Acad. Sci. USA **110**, 17195 (2013).
[24] N. Cabrera and M. M. Levine, Philos. Mag. **1**, 450 (1956).
[25] W. K. Burton, N. Cabrera, and F. C. Frank, Philos. Trans. R. Soc., A **243**, 299 (1951).
[26] Recently, Miura-Kobayashi [45] and Ohtsuka *et al.* [46] analytically and numerically studied the growth behavior of crystal surfaces driven by a group of multiple screw dislocations and directly compared the results with BCF theory [25].
[27] N. Cabrera and R. V. Coleman, *The Art and Science of Growing Crystals*, edited by J. J. Gilman (Wiley, New York, 1963).
[28] T. Surek, J. P. Hirth, and G. M. Pound, J. Cryst. Growth **18**, 20 (1973).
[29] T. Surek, G. M. Pound, and J. P. Hirth, Surf. Sci. **41**, 77 (1974).
[30] J. van der Eerden, J. Cryst. Growth **53**, 305 (1981).
[31] J. van der Eerden, J. Cryst. Growth **53**, 315 (1981).
[32] J. J. De Yoreo, T. A. Land, and J. D. Lee, Phys. Rev. Lett. **78**, 4462 (1997).
[33] M. J. McLoughlin, T. J. Mays, and R. Price, Phys. Rev. Lett. **95**, 115504 (2005).
[34] F. F. Liu, G. W. Yu, L. S. Zhang, L. Li, B. Wang, X. Y. Gan, H. K. Ren, H. L. Zhou, L. L. Zhu, S. H. Ji, M. X. Xu, B. A. Liu, X. G. Xu, Q. T. Gu, and X. Sun, Sci. Rep. **4**, 6886 (2014).
[35] A. Pimpinelli and J. Villian, *Physics of Crystal Growth*, edited by C. Godréche (Cambridge University Press, Cambridge, 1998).
[36] H. Asakawa, G. Sazaki, K. Nagashima, S. Nakatsubo, and Y. Furukawa, Cryst. Growth Des. **15**, 3339 (2015).
[37] H. Asakawa, G. Sazaki, K. Nagashima, S. Nakatsubo, and Y. Furukawa, Proc. Natl. Acad. Sci. USA **113**, 1749 (2016).
[38] K. Murata, H. Asakawa, K. Nagashima, Y. Furukawa, and G. Sazaki, Proc. Natl. Acad. Sci. USA **113**, E6741 (2016).
[39] B. van der Hoek, J. P. van der Eerden, and P. Bennema, J. Cryst. Growth **56**, 621 (1982).
[40] F. C. Frank, Acta Crystallogr. **4**, 497 (1951).
[41] P. V. Hobbs, *Ice Physics* (Oxford University Press, New York, 1974).
[42] The lateral side of the hollow core is expected to correspond to the prismatic face. Here we roughly set γ to be $0.1\,\mathrm{J/m^2}$ from Ref. [47] for an order of magnitude estimation.
[43] J. Heindl, H. P. Strunk, V. D. Heydemann, and G. Pensl, Phys. Status Solidi A **162**, 251 (1997).
[44] J. Heindl, W. Dorsch, H. P. Strunk, S. G. Müller, R. Eckstein, D. Hofmann, and A. Winnacker, Phys. Rev. Lett. **80**, 740 (1998).
[45] H. Miura and R. Kobayashi, Cryst. Growth Des. **15**, 2165 (2015).
[46] T. Ohtsuka, Y.-H. R. Tsai, and Y. Giga, Cryst. Growth Des. **18**, 1917 (2018).
[47] H. R. Pruppacher and J. D. Klett, *Microphysics of Clouds and Precipitation* (Kluwer Academic Publishers, Dordrecht, 1997).